International Journal on Interactive Design and Manufacturing (IJIDeM) (2022) 16:227–237
https://doi.org/10.1007/s12008-021-00824-7

ORIGINAL PAPER

Thermal simulation of wire arc additive manufacturing: a new material deposition and heat input modelling

Akram Chergui[1] · François Villeneuve[1] · Nicolas Béraud[1] · Frédéric Vignat[1]

Received: 27 January 2021 / Accepted: 18 December 2021 / Published online: 7 January 2022

Abstract
Wire arc additive manufacturing allows the production of metallic parts by the deposition of weld beads using arc-welding technologies. This low-cost additive manufacturing technology has the ability to manufacture large-scale parts at a high deposition rate. However, the quality of the obtained parts is greatly affected by the various thermal phenomena present during the manufacturing process. Numerical simulation remains an effective tool for studying such phenomena. In this paper, a new finite element method is proposed in order to model material deposition and heat input in WAAM process. This method allows to gradually construct the mesh representing the deposited zones along the deposition path. The heat source model from Goldak is adapted and combined with the proposed material deposition technique considering the power distribution between the filler material and the molten pool. The effectiveness of the new method is validated through a set of experimentations, one of which is detailed in this paper.

Keywords Wire-arc-additive-manufacturing · WAAM · Metal deposition · Finite element · Thermal behavior

1 Introduction

Additive manufacturing (AM) has experienced a remarkable growth over the last three decades, and its use is no longer limited to the production of prototypes, but is now extended to the direct manufacturing of functional metallic parts [1]. Today, Wire Arc Additive Manufacturing (WAAM) is one of the most promising direct energy deposition processes. Compared to other AM processes, this technology is inexpensive, offers a large workspace and allows for high productivity and energy efficiency. WAAM enables the production of metallic parts by depositing beads of welded metal, in a layer-by-layer manner, using arc-welding technologies. It combines an electrical arc as a heat source and a metal wire as feedstock. Welding torches are assembled on a positioning system as CNC milling machines or multi-axis robots [2]. WAAM shows considerable benefits compared to other additive and traditional manufacturing processes, especially for the manufacture of large and complex thin-walled structures. It allows high deposition rates (about 50–130 g/min compared to 2–10 g/min for electron beam or laser deposition [3]), but also the manufacturing of large-scale parts in a large workspace (theoretically there are no dimensional limits for the manufactured parts [4]). In addition, WAAM reduces manufacturing time by 40–60% and post-machining time by 15–20% depending on part size [5]… On the other hand, despite these promising advantages, the quality of parts manufactured by WAAM is greatly affected by various thermal phenomena occurring during the manufacturing process itself. For instance, the non-uniform temperature field experienced by the part during the deposition process, the constantly changing thermal conditions, heat accumulation and overheating phenomena, can lead to geometrical and material defects in the final part. It is well accepted in the literature that the quality of WAAM parts highly depends on their thermal history during the manufacturing process [5–7]. To guarantee the quality of parts, two approaches are possible: the first one is to implement experiments to adjust the process parameters, the other one considers AM simulation. Béraud et al. [8, 9] showed that process simulation remains an efficient tool for building a more thorough understanding of the different thermal phenomena involved in metal AM. This approach allows not only to reduce experimentation, but also to improve the process optimization, as well as the

✉ François Villeneuve
francois.villeneuve@grenoble-inp.fr

[1] Univ. Grenoble Alpes, Grenoble INP, G-SCOP, 46 avenue Felix Viallet, 38031 Grenoble, France

quality of the produced parts in a reduced time and at a lower cost.

Stavropoulos et al. [10] reviewed the different modeling approaches of AM processes, and highlighted the importance of modeling heat transfer related phenomena as it directly impacts the dimensional accuracy, topology, mechanical properties and microstructure of the final part. They also stated that numerical approaches remain the most suitable for modeling such phenomena, as they provide an overview of the physics throughout the process, requiring less assumptions compared to analytical approaches. Most recent work in AM literature addressed process simulation using finite element (FE) method. Xiong et al. [11, 12] studied the thermal behavior of cylindrical parts made by WAAM through a FE thermal simulation of the process. Other studies focused on improving efficiency and accuracy in FE modeling of WAAM process. Montevecchi et al. [13, 14] developed a FE model based on a mesh coarsening technique in order to reduce the computational cost of the process simulation. In the same perspective, Ding et al. [15] proposed a FE approach based on two models (transient and stationary) to investigate the thermomechanical behavior of parts manufactured in WAAM. Michaleris [16] reviewed the existing techniques for metal deposition modeling, and proposed a new hybrid algorithm for reducing the computational time. From the perspective of a simulation, WAAM process is very similar to multi-pass welding process [12]. However, the physics of welding process involves complex physical phenomena such as thermodynamics, heat and mass transfer, electricity and magnetism [17]. Modeling these phenomena at a part scale level can be very time consuming from a computational viewpoint. For this reason, most studies in literature recommend to model the heat input using a heat source model, prescribing a heat generation per unit volume, and taking into consideration the energy contribution of the different physical phenomena occurring in the molten pool. However, the set of FE models developed so far for WAAM process do not seem to be up to the task, for several reasons. First, it is still difficult to simulate an entire deposition strategy of a large-scale part in a reasonable time because of the substantial size of the mesh, and too numerous simulation time-steps to run. Secondly, the FE modeling techniques adopted in existing models, such as material deposition modeling techniques and boundary conditions simplification are prone to major errors.

That is why this paper proposes a FE model based on a new material deposition modeling technique and a new heat source model adapted from Goldak [18]. The aim is to model material and heat input in WAAM process simulation [19]. The proposed method allows not only to consider the energy distribution between the filler material and the molten pool, but also the boundary conditions change during the deposition process. The overall model is validated with an experimental test case, followed by outstanding results.

2 Proposed FE modeling for WAAM process

In FE simulation of AM processes and WAAM in particular, the pre-processing stage is required due to the layer-by-layer material deposition feature. This step takes into consideration various inputs that keep changing during the deposition process: the mesh, the heat input, the material properties and the boundary conditions, which requires specific modeling techniques. For this purpose, a FE model is proposed based on a new metal deposition modeling technique and an adapted heat source model. The main objective of this model is to incorporate the metal deposition feature of the process by considering the constantly evolving pre-processing inputs in the FE analysis of the deposition phase. The proposed model consists of three main steps, each modeling properly the material input, the heat input, the material properties and the boundary conditions, respectively. Each step includes a set of functions and procedures called between each two-time step in the deposition phase simulation, as illustrated in Fig. 1. These functions and procedures allow to update the pre-processing inputs at each deposition time-step, based on which the temperatures fields are calculated and stored successively. Consequently, the mesh representing the deposited layers as well as the corresponding temperature maps are constructed gradually according to the deposition path.

The model is implemented using the open-source FE code "Cast3M 2018". The post-processing stage, including results visualization and analysis, is performed using "ParaView" software.

2.1 Material deposition modeling

There are two traditional FE techniques for modeling material deposition in AM process simulation: inactive element method and quiet element method, as reviewed by Michaleris [16]. In the inactive element method, the elements representing the deposited regions are initially inactive, then activated gradually according to the deposition path. In the quiet element method, all elements are present from the start, but, as low values are assigned to their material properties (conductivity and specific heat), they do not affect the analysis. These material properties are then switched to the real values according to the deposition path. Both inactive and quiet methods can be used to model metal deposition in WAAM process, and have their advantages and drawbacks one to another. Quiet element method leads to a significant increase of the computational time. It considers the entire mesh size representing all layers to deposit from the start of the analysis. Inactive element method introduces errors into the FE analysis because of the artificial numerical thermal energy introduced during element activation. Furthermore, the interface between inactive (or quiet) and active elements is continuously evolving during the deposition phase. This

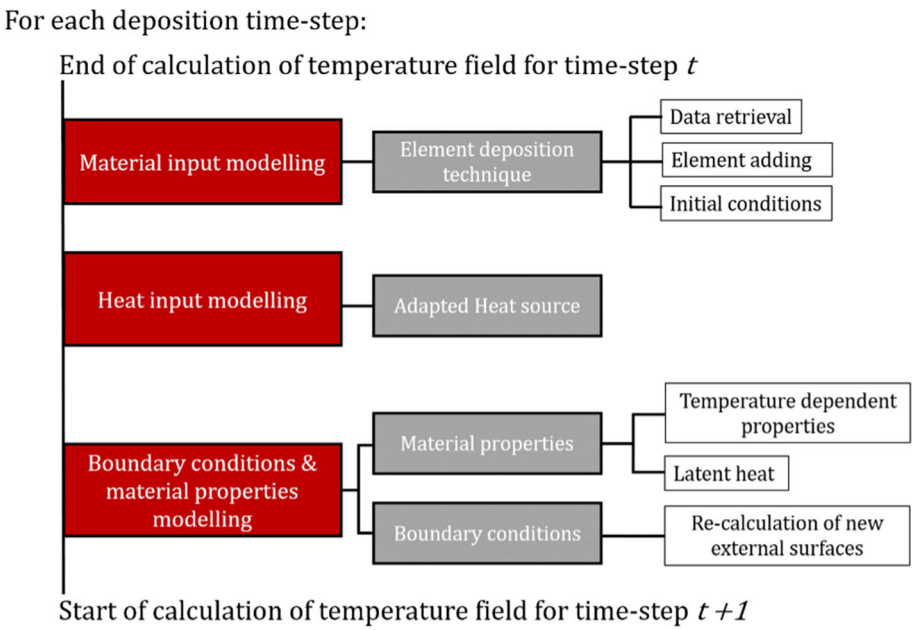

Fig. 1 Proposed FE model workflow for WAAM process

makes it difficult to compute this internal interface and consider its surface convection and radiation. For this reason, convection and radiation on this interface are neglected on both inactive and quiet element techniques but leads to additional errors in the FE analysis [16].

In the presented new model, metal deposition is considered using a new FE deposition technique. Each deposited droplet is indeed modeled by a set of elements, representing together a numerical droplet. Every numerical droplet is created at its corresponding time-step in the deposition phase simulation. The new created elements are then added to the previously created elements from last time-steps. Thus, the mesh representing the deposited regions is constructed gradually along the deposition path. This technique is implemented in the FE code through different functions and procedures that can be summarized in the following element deposition steps (Fig. 2).

At the end of the temperature field calculation for time-step t:

- "Data retrieval" consists in recovering the mesh as well as the temperature field, at the end of a given time-step t, used subsequently as input data at the next step.
- "Elements adding" creates a numerical droplet i.e. a set of elements representing the deposited droplet. These elements are added to the existing mesh at their corresponding position, as defined by the deposition path.
- "Initial conditions update" applies the previously retrieved temperature field to the mesh that represents the previously deposited regions and applies a uniform temperature field called T_d to the new deposited elements (see next section for evaluation of T_d).

The new constructed mesh and temperature field are selected as input for calculation of temperature field for time-step t + 1.

2.2 Heat input modeling

In order to model the heat input in welding process, Goldak et al. [18] proposed a volumetric heat source model in the form of a double-ellipsoidal, defined in a moving frame of reference, as shown in Fig. 3a. The model is defined by two Gaussian distributed power densities (Fig. 3b) allowing to better consider for heat distribution asymmetries in the molten pool. This model is expressed in Eq. 1.

$$\begin{cases} q_f(x,y,z) = \frac{6\sqrt{3}f_f Q}{\pi a_f bc\sqrt{\pi}} \exp\left(-3\frac{x^2}{a_f^2} - 3\frac{y^2}{b^2} - 3\frac{z^2}{c^2}\right) \\ q_r(x,y,z) = \frac{6\sqrt{3}f_r Q}{\pi a_r bc\sqrt{\pi}} exp\left(-3\frac{x^2}{a_r^2} - 3\frac{y^2}{b^2} - 3\frac{z^2}{c^2}\right) \end{cases} \quad (1)$$

$$f_f + f_r = 2 \quad (2)$$

$$Q = \eta U I \quad (3)$$

$$2Q = 2\eta U I = \int\int\int_{-\infty}^{+\infty} q(x,y,z)dxdydz \quad (4)$$

where q_f and q_r are the power density distributions in front and rear the center of the arc (origin of the frame of reference, as shown in Fig. 3a), respectively. b and c are the half-width (y semi-axis) and the depth (z semi-axis) of the source, a_f and a_r are the lengths of the front and rear ellipsoids (x semi-axes), respectively. f_f and f_r are the heat distribution factors of the front and rear ellipsoids, and can have different values, provided to respect the condition expressed in Eq. 2. Q is the

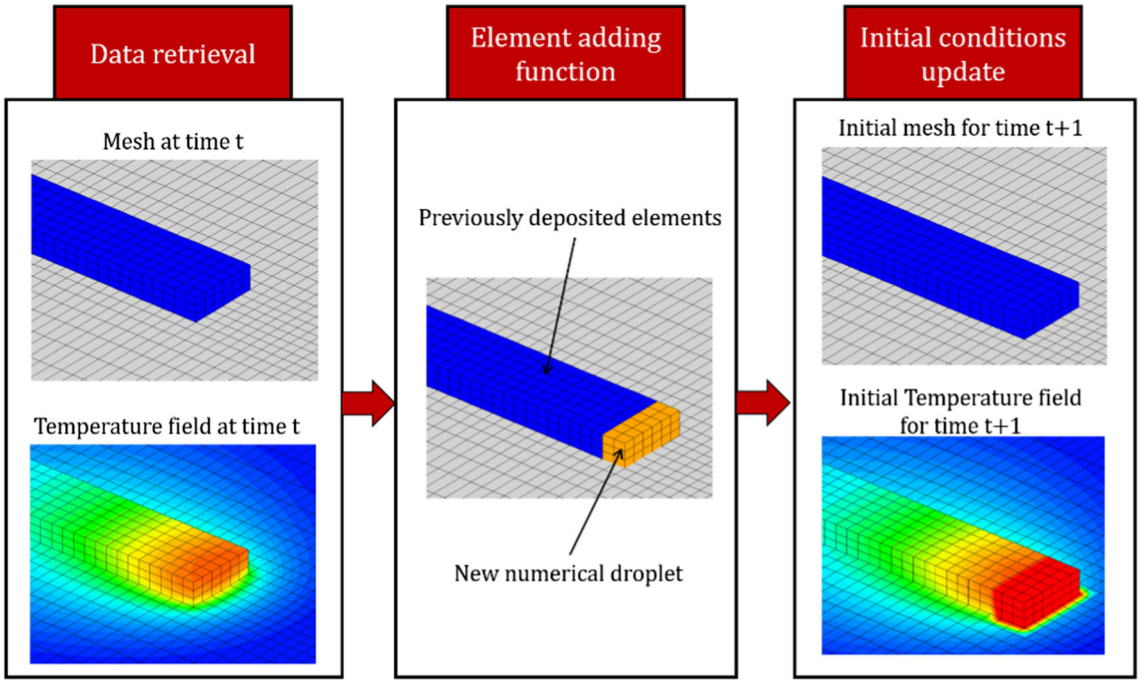

Fig. 2 Main steps of element deposition technique

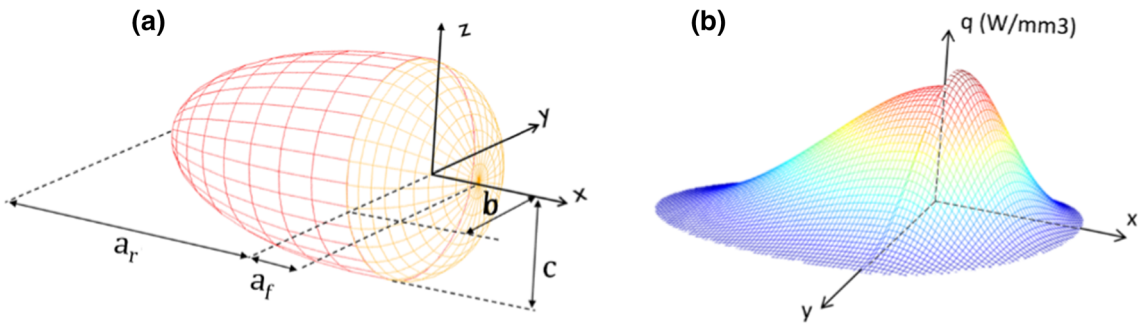

Fig. 3 Goldak double-ellipsoidal heat source (adapted from [18])

total power supplied by the arc, and is expressed in Eq. 3 as the product of welding current I, welding voltage U, and arc efficiency η. It is easy to show the relationship defined in Eq. 4.

The double-ellipsoidal heat source model has been widely used for modeling heat input in welding simulation, and is still relevant in WAAM process simulation. However, in order to use it in the new present deposition model, this sophisticated heat source needs to be adapted and further developed. In WAAM, the arc power is not fully delivered to the part directly. According to previous works, about 50% of the total arc power is used to melt the feed wire. This energy is subsequently transmitted to the part through the enthalpy of the deposited droplet [12, 20].

In the present model, the Goldak heat source is adapted and combined with the proposed element deposition technique for modeling the heat input in WAAM process. It takes into consideration the energy distribution between the wire and the substrate. In fact, the direct energy transfer from the arc to the substrate is considered using the inferior half of the double-ellipsoid Goldak model. The remaining 50% of the total energy is delivered by means of the deposited elements (Fig. 4). These latter are charged with an amount of energy equivalent to the energy delivered by the adapted heat source, as expressed in Eq. 5.

$$Q_{source} = Q_{elements} = \frac{\eta U I}{2} \tag{5}$$

The energy $Q_{elements}$ attributed to the deposited numerical droplet is expressed as a uniform temperature field imposed on the elements representing the deposited droplet. The value of the deposition temperature is calculated in Eq. 6.

$$T_d = \frac{\eta U I \Delta t}{2 \rho V C_p} + T_{ini} \tag{6}$$

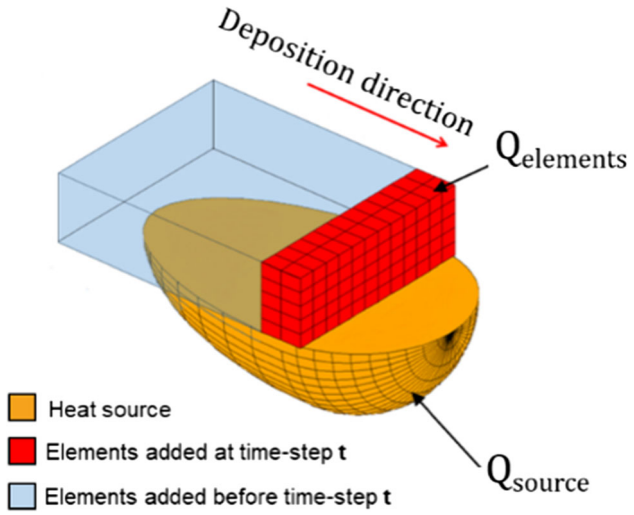

Fig. 4 Adapted Goldak heat source

where T_d is the deposition temperature, Δt is the value of the deposition time-step, V, ρ are the volume and density of the deposited element respectively (where ρV remains constant whatever the temperature), C_p is the average of the material specific heat capacities of the deposited elements and T_{ini} is the initial temperature of the welding wire. The reason why latent heat is not considered in this formula is explained at the end of paragraph 2.3.

This adapted model could be proposed thanks to the element deposition technique, which enables to properly simulate the wire melting energy transferred to the molten pool by means of the deposited droplets enthalpy. In addition, it helps to position correctly the heat source origin along z and x axes according to the deposited elements, thus simulating the molten pool properly.

2.3 Boundary conditions and material properties modeling

As discussed earlier, the internal interface between inactive (or quiet) and active elements is difficult to compute, because it changes continuously during the deposition phase. Therefore, when using inactive or quiet element methods, surface convection and radiation are often neglected on the internal interface, but introduce errors to the FE analysis. It is easier to overcome such issue by using the proposed element deposition technique, as the internal active/inactive interface becomes an external free surface, as shown Fig. 5b. In the proposed simulation, a model-update procedure is developed in order to implement the element deposition technique properly. This procedure is called after each deposition time-step, and updates the following pre-processing inputs of the FE analysis. It allows to compute the external surface of the total mesh and to update convection and radiation heat loads according to the new obtained external mesh surface (Fig. 5a). The evolution of material properties such as conductivity, specific heat and density as a function of temperature is also taken into consideration.

During the deposition process, the deposited material undergoes multiple heating and cooling cycles that result in a local phase change from solid to liquid during melting, and from liquid to solid during solidification. To consider the latent heat during the FE analysis of an entire deposition strategy presents many problems in terms of simulation convergence and computational time. Two phase change modeling techniques were tested in this work, namely: the heat counting method proposed by Cast3M, and the specific heat artificial variation technique. These two techniques do not ensure the convergence of the simulation with "Cast3M 2018", even when using extremely short computing time-steps. For this reason, an alternative method is proposed. The basic idea of this method is not to model the phase change during the FE calculation, but rather to readjust the obtained temperature maps according to the latent heat. In a first step, the deposition strategy is simulated entirely using the FE simulation without considering the latent heat, and the temperature fields of all-time steps are stored. In a second step, the previously calculated temperature fields are processed by a C++ code readjusting the temperatures exceeding solidus temperature, at each single node, as a function of latent heat, as shown in Fig. 6. This method allows results in a more stable and faster simulation.

3 Validation

In order to check the effectiveness of the proposed simulation model, an experimental validation was carried out by comparing simulated and experimental thermal curves of a test case. The test case consists in fabricating two thin-wall parts of eight layers according to two different strategies: raster and zigzag (Fig. 7). The test case parts dimensions are 80 mm in length and 6 mm in width, and the base plate dimensions are 250 mm in length and width, and 5 mm in thickness, as illustrated in Fig. 7.

The choice of the two test cases is motivated by the following reasons. Since we are in a WAAM context, most of the shapes realized are combinations of thin walls, hence the choice of this geometry. In order to vary some parameters, two strategies (raster or zigzag) and two idle time (idle time of 2 or 3.5 s) are considered. Limiting the tests to 8 layers allows to obtain experimental and simulation results in reasonable times while integrating dynamic phenomena. It should also be noted that the long-term objective of these simulations is to build thermal indicators, allowing to validate manufacturing strategies leading to good part geometries, but not to make a sharp prediction of the temperature dynamics in order to

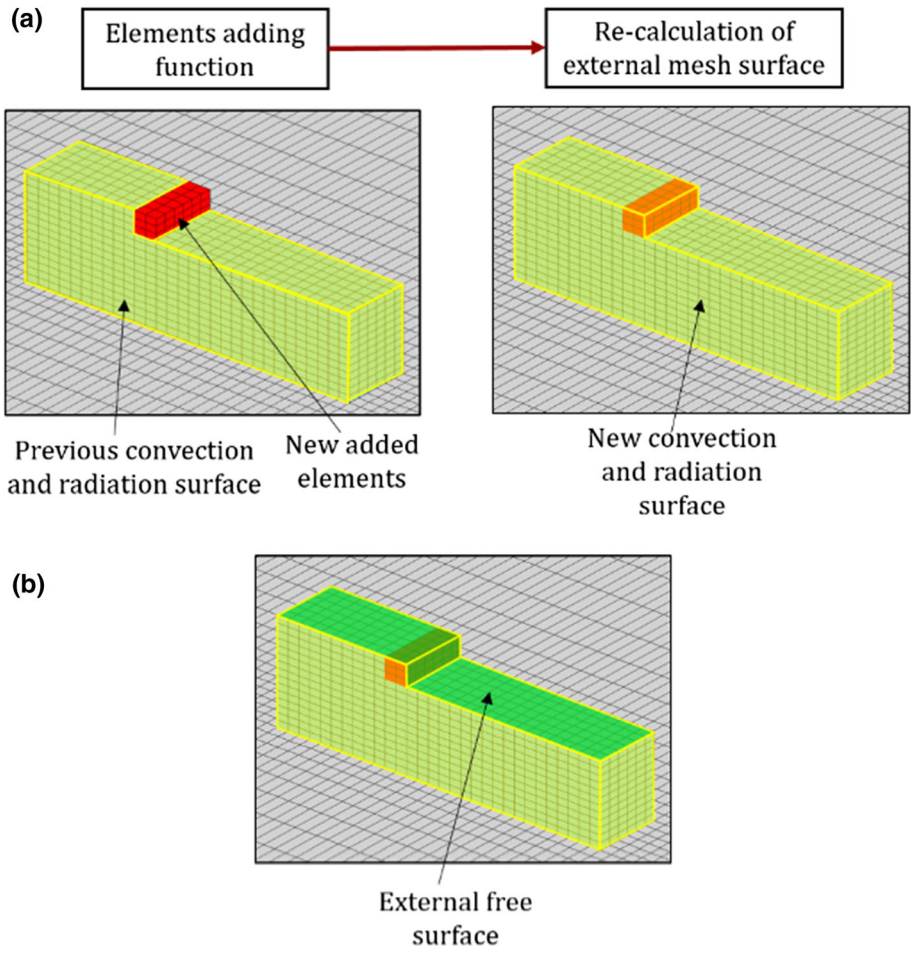

Fig. 5 External surface recalculation

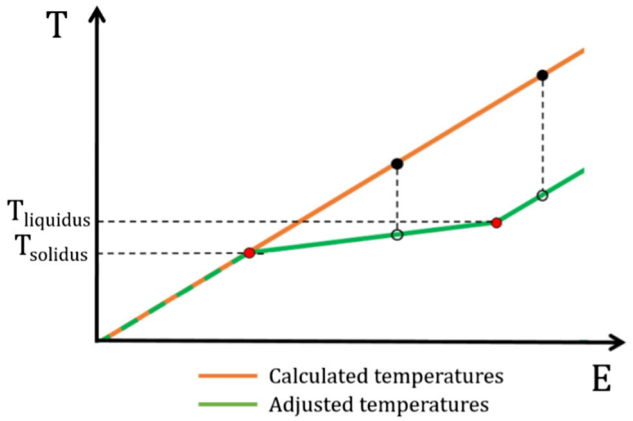

Fig. 6 Corrected temperatures to integrate latent heat

analyze metallurgical characteristics for example. Therefore, the chosen test cases should allow for the proper validation of the proposed model.

The test case was carried out using a WAAM cell including a Fronius CMT welding torch mounted on a Yaskawa MA1440 six-axis robot, and a two-axis positioner. Details of both deposition strategies (Raster and Zigzag) are presented in Table 1.

Two different materials have been considered in this experiment. The substrate plate material was an AA5083 welding aluminum alloy, and the thin-walls structures were manufactured using an AA5356 aluminum alloy filler wire with a diameter of 1.2 mm. The beads were deposited under a 100% argon gas protection with a flow rate of 13L/min.

Due to the similarities between these two alloys and in the absence of technical data in the literature regarding the temperature dependent material properties of AA5356, the properties of AA5083 are considered for both base and filler metals. Their values obtained from [21] are presented in Table 2.

During the manufacturing process (deposition and cooling phases), temperatures as function of time were measured at six different points (P1 to P6) on the substrate plate, as illustrated in Fig. 7, using six k-type thermocouples whose characteristics are presented in Table 3.

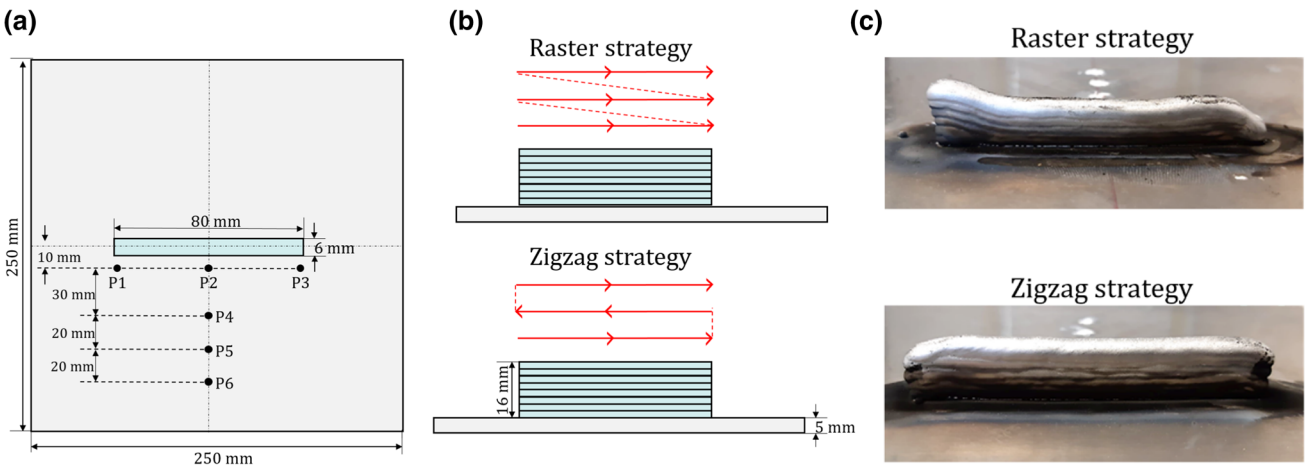

Fig. 7 Experimental design: xy view (**a**); xz view, raster and zigag strategies (**b**); produced parts (**c**)

Table 1 Test-case strategies parameters

Deposition trajectory	Welding current (A)	Welding voltage (V)	Travel speed (mm/s)	Wire feed speed (m/min)	Idle-time (s)
Raster	12	80	10	5	3.5
Zigzag	12	80	10	5	2

Table 2 Temperature-dependent material properties of aluminum alloy 5083 (from [21])

Temperature (°C)	25	80	180	280	380	480	580
Conductivity (W/m °C)	120	122.7	131.6	142.3	152.5	159.5	177.2
Specific heat (J/Kg °C)	924.1	984.2	1039.6	1081.2	1137.6	1178.2	1261.4
Density (Kg/m3)	2673.9	2642.7	2629.4	2611.5	2589.3	2567	2549

Table 3 K-type thermocouples characteristics

Precision (°C)	Measurement range (°C)	Sample rate (Hz)
±2.2	[− 200, 1250]	10

Table 4 Heat source parameters

Parameters	Q (W)	η	a_f (mm)	a_r (mm)	b (mm)	c (mm)
Values	960	0.83	3	6.5	3	3

3.1 Test case simulation

The test case parts were simulated using the proposed FE simulation. The overall mesh, including both base plate and deposited elements, contains 57,270 8-nodes brick elements. The adapted heat source semi-axes used in the simulation are calibrated using the macro-scratch patterns of the molten pool as recommended by Goldak et al. [18], and their values are presented in Table 4.

In the simulation post-processing stage, the evolution of the mesh and the corresponding temperature field can be visualized. The simulated temperature fields at the first, second, seventh and the eighth layers are illustrated in Fig. 8 (zigzag strategy as an example). The temperature curves as a function of time are extracted from the nodes representing the control points P1–P6. The simulation of each strategy requires about 3 h on a personal computer.

3.2 Results and discussion

Figure 9 presents the experimental temperature curves as a function of time at points P1, P2 and P3, compared to the results obtained with the proposed simulation. Comparison for both Raster and Zigzag strategies are shown in Fig. 9.(a) and Fig. 9.(b), respectively.

The results show that the simulated and the experimental temperature curves at control points P1, P2 and P3 are correlated with good agreement. Moreover, during the deposition phase of the Raster strategy, eight peaks can be observed on both experimental and numerical curves, as shown in Fig. 9.a. These peaks represent the eight passages of the heat source near control points P1, P2 and P3. In the Zigzag strategy, a set of four peaks composed of two successive vertices each, are recorded on the curves corresponding to control points P1 and P3. At these points, the torch quickly passes and returns to the same end point. The reason is to initiate the

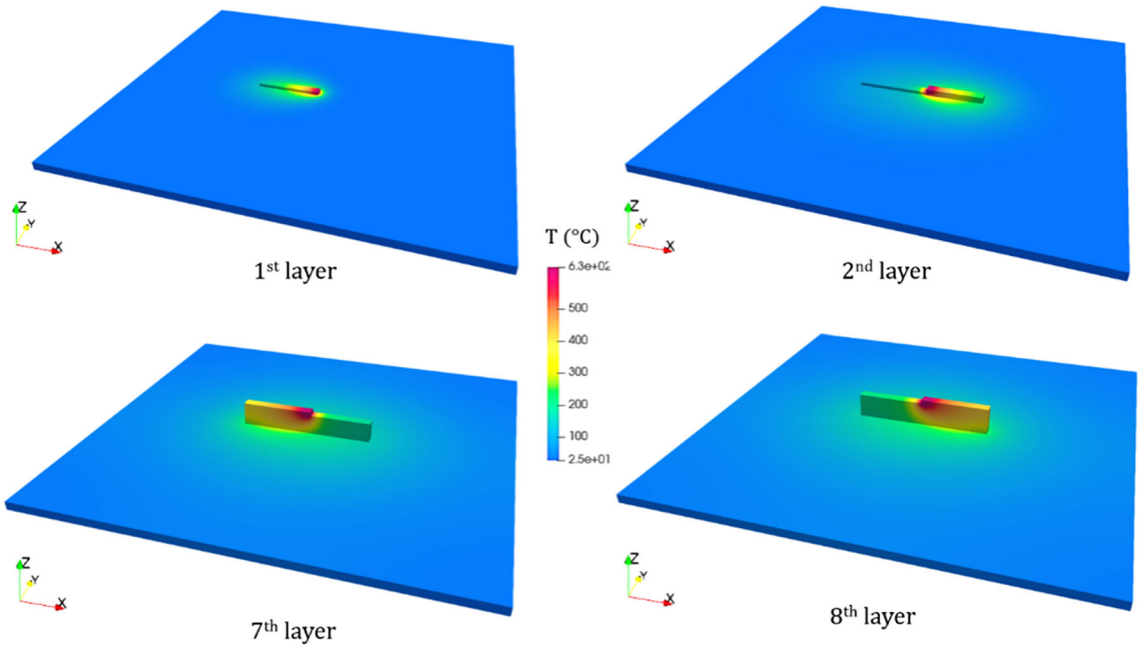

Fig. 8 Simulated temperature field of Zigzag strategy at different layers

deposition of the next layer, leaving little time for cooling, which explains the two successive vertices. This detail was not only measured by thermocouples, but was also obtained by simulation.

A good agreement is also achieved between the experimental and numerical temperature curves at control points P4, P5, and P6 (y-axis direction) for both strategies, as shown in Fig. 10. In this direction, it is quite normal not to distinguish the eight temperature peaks on the curves, given the important distance between these control points and the deposited layers.

The position of the peaks as a function of time can be explained as follows.

Concerning the raster strategy, given the travel speed fixed at 10 mm.s-1, the part length fixed at 80 mm and the idle time fixed at 3.5 s, each new layer starts every $80/10 + 3.5 = 11.5$ s. There is a time lag between the passage of the welding torch in front of the sensors and the maximum temperature reached by this sensor (the different peaks) due to the distance of the sensors from the wall. For example, sensors P1, P2 and P3 are 10 mm from the wall. Thus the 8th layer starts at $t = 80.5$ s and then the last 3 peaks for the sensors P1, P2 and P3 appear after 80.5 s.

Concerning the zigzag strategy, each new layer starts every 10 s because of the idle time of 2 s. The last layer starts at $t = 70$ s and thus the last peaks of the sensors appear after 70 s.

The progressive increase in temperature is due to the relatively short idle time. This causes the part to accumulate heat with each layer. This means that each new temperature peak is higher than the previous one.

The average errors between simulated and experimental values has been calculated for each of the sensors and for both strategies, Raster and Zigzag (Table 5). This average error remains mostly below 10.5% for the three closest sensors with a better correlation in the Raster case (less than 7.3% error) than in the Zigzag case (less than 10.6% error). This difference can be explained by the more important dynamics of the phenomena in the Zigzag case because of the back and forth movement of the welding torch alternately at points P1 and P3.

The correlation between experimentation and simulation tends to be reinforced as the layers go on, which validates the initial choice of a limited number of layers, and is sufficient to validate the model. However, the gap is higher in the early peaks. Possible sources of such error could be the thermal inertia of the thermocouples. But all in all, these correlations provide further validation on the effectiveness of the proposed model.

4 Conclusion

In this study, a thermal FE model is proposed for WAAM process based on a new material deposition technique and an adapted heat source model. The major outcomes of this model can be summarized by the following features:

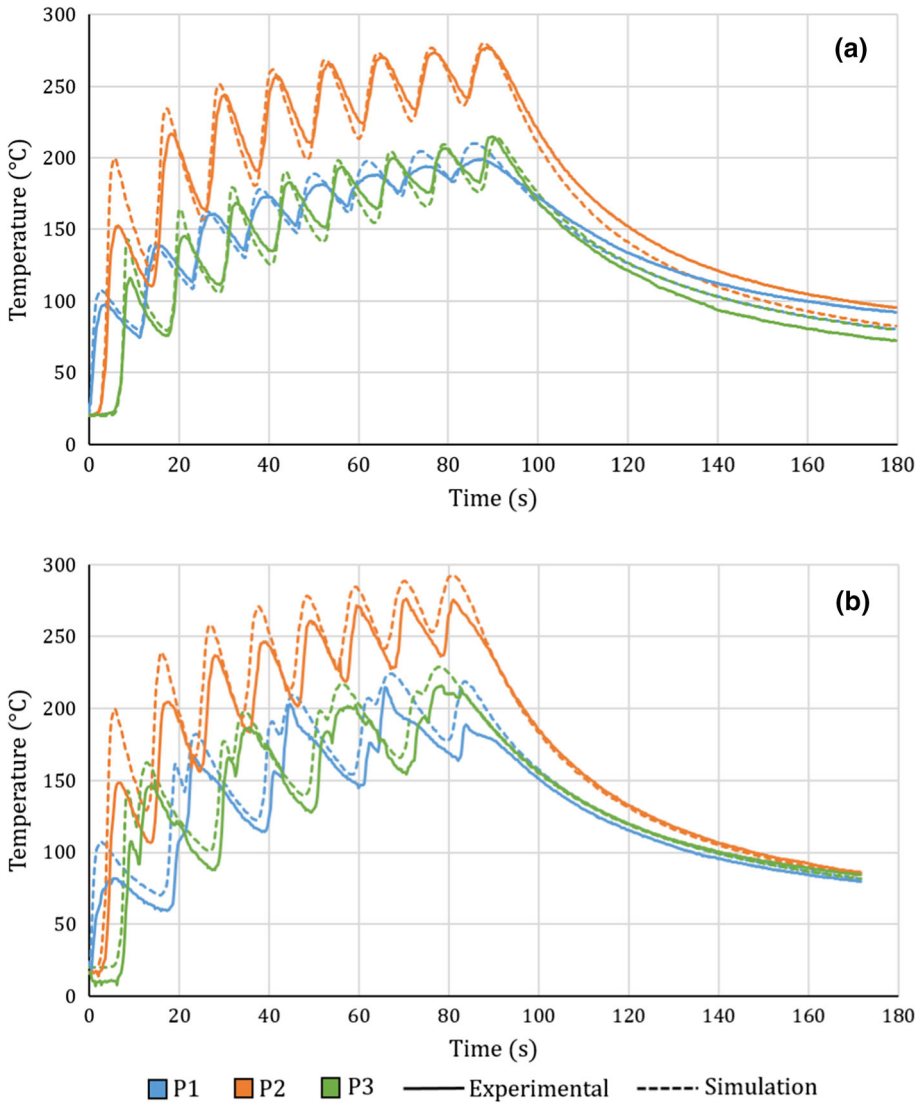

Fig. 9 Comparison of simulated and experimental temperature curves at P1, P2 and P3 for Raster (**a**) and Zigzag (**b**) strategies

- A new FE deposition technique
- An adaptation of the Goldak heat source
- A better integration of the heat exchanges by the external surfaces
- A good ratio between calculation time and accuracy of results

This element deposition technique enables, for each deposition time-step, to add new elements to the previous mesh, following the passage of an adapted heat source. Thus, it helps to model both material and heat input, and to better consider heat exchange in the external surfaces. The proposed modeling technique is validated through an experimental test case, where simulated results agree with the experimental curves. Indeed, the differences between experimentation and simulation are between 5 and 10% for a reasonable calculation time of about 3 h for a wall of 80 mm long on 8 layers. Thanks to the proposed FE modeling techniques, it is possible to simulate the thermal history of an entire WAAM deposition strategy with sufficient precision, and within a reasonable time.

In the future, the proposed simulation is to be used for the development of a set of thermal quality criteria. This would support the evaluation of the quality of WAAM fabricated parts, and hence their deposition strategies. From these criteria, WAAM deposition strategies could be optimized and the quality of the fabricated parts would be enhanced by integrating optimization algorithms into the simulation. A paper is in the process of being written to present the first results obtained in that direction. In the long term, this work should also allow to establish correlations between the simulated thermal maps and the geometrical characteristics of the pro-

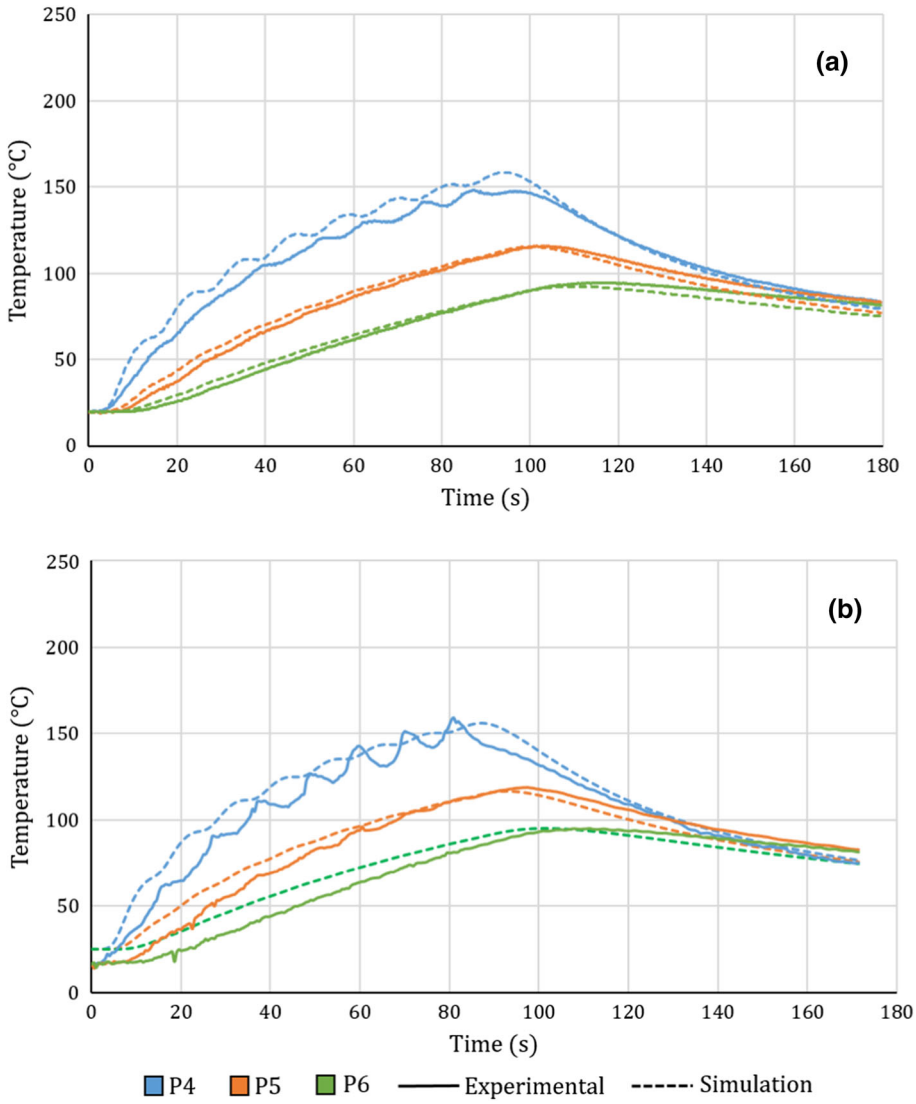

Fig. 10 Comparison of simulated and experimental temperature curves at P4, P5 and P6 for Raster (**a**) and Zigzag (**b**) strategies

Table 5 Average errors between simulated and measured, in percentage of the measured value

Deposition trajectory	P1 (%)	P2 (%)	P3 (%)	P4 (%)	P5 (%)	P6 (%)
Raster	5.8	7.3	6.1	6	5.1	5.2
Zigzag	10.4	8	10.6	8.9	12.7	17

duced parts. In particular, a research about the links between process parameters and resulting geometrical shapes as for example in [22] seems promising.

Funding The work presented was funded by Univ. Grenoble Alpes.

Declarations

Conflicts of interest The author declare that they have no conflict of interest.

References

1. Vayre, B., Vignat, F., Villeneuve, F.: Metallic additive manufacturing: state-of-the-art review and prospects. Mech. Ind. **13**(2), 89–96 (2012). https://doi.org/10.1051/meca/2012003
2. Lopes Nunes, M., Pereira, A.C., Alves, A.C.: Smart products development approaches for industry 4.0. Proced. Manuf. **13**, 1215–1222 (2017). https://doi.org/10.1016/j.promfg.2017.09.035
3. Liberini, M., et al.: Selection of optimal process parameters for wire arc additive manufacturing. Proced. CIRP **62**, 470–474 (2017). https://doi.org/10.1016/j.procir.2016.06.124
4. Derekar, K.S.: A review of wire arc additive manufacturing and advances in wire arc additive manufacturing of aluminium. Mater. Sci. Technol. **34**(8), 895–916 (2018). https://doi.org/10.1080/02670836.2018.1455012

5. Zhao, Y., Jia, Y., Chen, S., Shi, J., Li, F.: Process planning strategy for wire-arc additive manufacturing: thermal behavior considerations. Addit. Manuf. **32**, 100935 (2020). https://doi.org/10.1016/j.addma.2019.100935
6. Montevecchi, F., Venturini, G., Grossi, N., Scippa, A., Campatelli, G.: Heat accumulation prevention in wire-arc-additive-manufacturing using air jet impingement. Manuf. Lett. **17**, 14–18 (2018). https://doi.org/10.1016/j.mfglet.2018.06.004
7. Wang, Z., Zimmer-Chevret, S., Léonard, F., et al.: Prediction of bead geometry with consideration of interlayer temperature effect for CMT-based wire-arc additive manufacturing. Weld. World **65**, 2255–2266 (2021). https://doi.org/10.1007/s40194-021-01192-2
8. Béraud, N., Vignat, F., Villeneuve, F., Dendievel, R.: Improving dimensional accuracy in EBM using beam characterization and trajectory optimization. Addit. Manuf. **14**, 1–6 (2017). https://doi.org/10.1016/j.addma.2016.12.002
9. Vignat, F., Béraud, N., Villeneuve, F.: Rapid thermal simulation of powder bed additive manufacturing.In: 2018 IEEE International Conference on Industrial Engineering and Engineering Management (IEEM), pp. 1498–1502. Bangkok, (2018), doi: https://doi.org/10.1109/IEEM.2018.8607695
10. Stavropoulos, P., Foteinopoulos, P.: Modelling of additive manufacturing processes: a review and classification. Manuf. Rev. **5**, 2 (2018). https://doi.org/10.1051/mfreview/2017014
11. Xiong, J., Lei, Y., Li, R.: Finite element analysis and experimental validation of thermal behavior for thin-walled parts in GMAW-based additive manufacturing with various substrate preheating temperatures. Appl. Therm. Eng. **126**, 43–52 (2017). https://doi.org/10.1016/j.applthermaleng.2017.07.168
12. Xiong, J., Li, R., Lei, Y., Chen, H.: Heat propagation of circular thin-walled parts fabricated in additive manufacturing using gas metal arc welding. J. Mater. Process. Technol. **251**, 12–19 (2018). https://doi.org/10.1016/j.jmatprotec.2017.08.007
13. Montevecchi, F., Venturini, G., Scippa, A., Campatelli, G.: Finite element modelling of wire-arc-additive-manufacturing process. Proced. CIRP **55**, 109–114 (2016). https://doi.org/10.1016/j.procir.2016.08.024
14. Montevecchi, F., Venturini, G., Grossi, N., Scippa, A., Campatelli, G.: Finite element mesh coarsening for effective distortion prediction in wire arc additive manufacturing. Addit. Manuf. **18**, 145–155 (2017). https://doi.org/10.1016/j.addma.2017.10.010
15. Ding, J., et al.: Thermo-mechanical analysis of wire and arc additive layer manufacturing process on large multi-layer parts. Comput. Mater. Sci. **50**(12), 3315–3322 (2011). https://doi.org/10.1016/j.commatsci.2011.06.023
16. Michaleris, P.: Modeling metal deposition in heat transfer analyses of additive manufacturing processes. Finite Elem. Anal. Des. **86**, 51–60 (2014). https://doi.org/10.1016/j.finel.2014.04.003
17. Hu, J., Tsai, H.L.: Heat and mass transfer in gas metal arc welding. Part I: the arc. Int. J. Heat Mass Transf. **50**(5–6), 833–846 (2007). https://doi.org/10.1016/j.ijheatmasstransfer.2006.08.025
18. Goldak, J., Chakravarti, A., Bibby, M.: A new element model for welding heat source. Metall. Mater. Trans. B **15**, 299–305 (1984). https://doi.org/10.1007/BF02667333
19. Chergui, A., Beraud, N., Vignat, F., Villeneuve, F.: Finite element modeling and validation of metal deposition in wire arc additive manufacturing. In: Roucoules, L., Paredes, M., Eynard, B., Morer Camo, P., Rizzi, C. (eds.) Advances on mechanics, design engineering and manufacturing III. JCM 2020. Lecture notes in mechanical engineering. Springer, Cham (2021). https://doi.org/10.1007/978-3-030-70566-4_11
20. DuPont, J.N., Marder, A.R.: Thermal efficiency of arc welding processes. Weld. J.-Incl. Weld. Res. Suppl. **74**(12), 406s-416s (1995)
21. El-Sayed, M.M., Shash, A.Y., Abd-Rabou, M.: Finite element modeling of aluminum alloy AA5083-O friction stir welding process. J. Mater. Process. Technol. **252**, 13–24 (2018). https://doi.org/10.1016/j.jmatprotec.2017.09.008
22. Manokruang, S., Vignat, F., Museau, M., Limousin, M.: Process parameters effect on weld beads geometry deposited by wire and arc additive manufacturing (WAAM). In: Roucoules, L., Paredes, M., Eynard, B., Morer Camo, P., Rizzi, C. (eds.) Advances on mechanics, design engineering and manufacturing III. JCM 2020. Lecture notes in mechanical engineering. Springer, Cham (2021)